Earth Surface Processes and Landforms
Earth Surf. Process. Landforms **30**, 985–1006 (2005)
Published online in Wiley InterScience (www.interscience.wiley.com). **DOI:** 10.1002/esp.1258

Rates of erosion and topographic evolution of the Sierra Nevada, California, inferred from cosmogenic ^{26}Al and ^{10}Be concentrations

Greg M. Stock,[1]* Robert S. Anderson[1,2] and Robert C. Finkel[3]
[1] *Department of Earth Sciences, University of California, Santa Cruz, CA 95064, USA*
[2] *Department of Geological Sciences and Institute of Arctic and Alpine Research, University of Colorado, Boulder, CO 80309, USA*
[3] *Center for Accelerator Mass Spectrometry and Geosciences and Environmental Technology, Lawrence Livermore National Laboratory, Livermore, CA 94550, USA*

**Correspondence to: G. M. Stock, Department of Geological Sciences, University of Michigan, Ann Arbor, MI 48109-1005, USA. E-mail: gstock@umich.edu*

Received 1 September 2004; Revised 28 February 2005; Accepted 17 March 2005

Abstract

Concentrations of cosmogenic ^{26}Al and ^{10}Be in cave sediments and bedrock surfaces, combined with studies of landscape morphology, elucidate the topographic history of the southern Sierra Nevada over the past 5 Ma. Caves dated by ^{26}Al/^{10}Be in buried sediments reveal that river incision rates were moderate to slow between *c.* 5 and 3 Ma ($\leq$0·07 mm a^{-1}), accelerated between 3 and 1·5 Ma (*c.* 0·3 mm a^{-1}), and then have subsequently become much slower (*c.* 0·02 mm a^{-1}). Although the onset of accelerated incision coincides in time with both postulated Pliocene tectonism and pronounced global climate change, we argue that it primarily represents the response to a discrete tectonic event between 3 and 5 Ma. Dated cave positions reveal that, prior to 3 Ma, river canyons displayed up to 1·6 km of local relief, suggesting that Pliocene rock uplift elevated pre-existing topography. Renewed incision beginning *c.* 3 Ma deepened canyons by up to 400 m, creating narrow inner gorges. Tributary streams exhibit strong convexities, indicating that the transient erosional response to Pliocene uplift has not yet propagated into upland surfaces. Concentrations of ^{26}Al and ^{10}Be in bare bedrock show that upland surfaces are eroding at slow rates of *c.* 0·01 mm a^{-1}. Over the past *c.* 3 Ma, upland surfaces eroded slowly while adjacent rivers incised rapidly, increasing local relief. Although relief production probably drove at least modest crestal uplift, considerable pre-Pliocene relief and low spatially averaged erosion rates suggest that climatically driven rock uplift is not sufficient to explain all uplift implied by tilted markers at the western edge of the range. Despite the recent pulse of erosion, spatially averaged erosion rates are low, and have probably acted to preserve the broad topographic form of the Sierra Nevada throughout much of the late Cenozoic.

Keywords: cosmogenic nuclides; burial ages; bedrock incision; relief; landscape evolution; Sierra Nevada

Introduction

The evolution of mountainous topography results from complex interactions between tectonic forces and climatically driven erosion. The relative roles these factors have played in the apparent uplift and erosion of mountain belts in the late Cenozoic remains a topic of debate (e.g. Molnar and England, 1990; Raymo and Ruddiman, 1992; Zhang *et al.*, 2001). Many studies have focused on the Sierra Nevada range of California, where postulated tectonic uplift in the past 3 to 5 million years (Ma) coincided with pronounced global climate change. These studies have suggested either fundamentally tectonic (e.g. Unruh, 1991; Wakabayashi and Sawyer, 2001; Jones *et al.*, 2004) or climatic (Small and Anderson, 1995) mechanisms for uplift, while others call for no late Cenozoic uplift at all and a reduction of altitude (Wernicke *et al.*, 1996; House *et al.*, 1998; Poage and Chamberlain, 2002). Spatially and temporally distributed erosion rates, particularly from the rugged southern Sierra, can help to test the postulated uplift hypotheses and clarify the roles tectonics and climate play in the evolution of mountainous topography.

Cosmogenic nuclides offer unprecedented insights into rates of mountain erosion. For example, nuclide concentrations record long-term erosion rates of bare bedrock surfaces (e.g. Lal, 1991; Small *et al*., 1997; Bierman and Caffee, 2002), and can be used to date strath terraces (Burbank *et al*., 1996; Reusser *et al*., 2004). Nuclide concentrations in alluvial sediment can date depositional terraces (Hancock *et al*., 1999; Hanks *et al*., 2004; Wolkowinsky and Granger, 2004), and yield catchment-averaged erosion rates (e.g. Granger *et al*., 1996; Bierman and Steig, 1996; Schaller *et al*., 2001, 2002; Vance *et al*., 2003). If previously exposed sediment is deeply buried, differential decay between two nuclides can date the time of burial (e.g. Granger and Muzikar, 2001; Granger *et al*., 1997, 2001b). Together these applications can reveal much about the timing and magnitude of topographic evolution in mountainous regions.

In the Sierra Nevada, a unique juxtaposition of riverside marble caves inset below granitic upland surfaces provides an opportunity to integrate multiple cosmogenic nuclide techniques to determine erosion rates across diverse landforms. We dated caves in canyon walls using $^{26}Al/^{10}Be$ burial dating to document rates of river incision into bedrock, a primary means by which landscapes respond to tectonic forcing. We also measured nuclide concentrations in bare bedrock surfaces to constrain erosion rates of adjacent granitic uplands. By combining these techniques, we derive high-resolution records of erosion, relief production, and palaeotopography in the Sierra Nevada over the past 5 Ma. These new records help to link many of the conceptual models put forth to explain the modern topography.

The Sierra Nevada

The Sierra Nevada is an asymmetric, west-tilted fault block with a mean altitude of *c*. 2800 m and crestal altitudes up to 4419 m. It is flanked on the west by the Great Valley, a deep structural basin, and on the east by the extensional Basin and Range Province (Figure 1A). Due to the tilt-block geometry, the range crest is skewed to the east, and the eastern slope is a steep normal-faulted escarpment. Below the glacially sculpted cirques and arêtes of the range crest, the broad western slope of the range descends in a series of undulating low-relief upland surfaces punctuated by deeply incised river canyons (Figures 1A and 2). As the Great Valley is thought to have remained at sea level throughout the Cenozoic (Huber, 1981), differential rock uplift between the Great Valley and the range crest (i.e. westward tilting) has been accomplished about a hinge line in the eastern Great Valley (Figure 1A). Differential rock and surface uplift are greatest at the range crest; in this paper, crestal uplift is synonymous with maximum uplift. While the northern Sierra represents a simple westward-tilted block, the southern Sierra displays a more complex westward-stepping pattern that also dips to the south (Bateman and Wahrhaftig, 1966; Wakabayashi and Sawyer, 2001).

Cretaceous arc volcanism apparently built high-standing topography that was deeply eroded in the early Cenozoic. Presently exposed rocks in the range are predominantly late Cretaceous (*c*. 80–120 Ma) granitic rocks of the Sierra Nevada batholith (e.g. Chen and Moore, 1982) that intruded Jurassic to Triassic country rocks that now fringe the batholith as fragmented metamorphic pendants (Figure 1A). Eocene sediments locally cover plutons aged *c*. 100 Ma emplaced at depths of 11 to 15 km (Ague and Brimhall, 1988), requiring erosion rates averaging 0·26–0·35 mm a^{-1} between roughly 100 and 40 Ma. Correspondingly, sedimentation rates in the Great Valley between 100 and 40 Ma are as high as 0·52 mm a^{-1}. However, Oligocene and Miocene–Pliocene deposits set into Eocene sediments suggest minimal river incision at exceptionally low rates (<0·003 mm a^{-1}) after *c*. 40 Ma, corresponding to sustained low sedimentation rates of 0·02 mm a^{-1} (Wakabayashi and Sawyer, 2001). Renewed volcanism beginning *c*. 15 Ma resulted in nearly continuous cover of the northern Sierra by about 5 Ma (Figure 1; Bateman and Wahrhaftig, 1966). Incision through these deposits yields time-averaged rates of 0·15 mm a^{-1} over the past 5 Ma, corresponding to Great Valley sedimentation rates of 0·16 mm a^{-1} (Wakabayashi and Sawyer, 2001).

Much of the debate presently surrounding the Sierra Nevada relates to whether the range experienced renewed tectonism in the late Cenozoic. A Miocene to early Pleistocene age for creation of modern topography has long been advocated based on apparently tilted river channels (e.g. Lindgren, 1911). Subsequent detailed analyses of tilted channels, volcanic flows, and Great Valley strata along the western slope refined estimates of the timing and magnitude of rock uplift at the crest; projection of tilted markers along a rigid block suggests *c*. 1·5 to 2·5 km of crestal rock uplift over the last 10 Ma, with most uplift occurring in the past 3 to 5 Ma (Huber, 1981; Unruh, 1991; Wakabayashi and Sawyer, 2001; Jones *et al*., 2004). Renewed tectonism from 3 to 5 Ma is supported by incision through volcanic deposits and accelerated Great Valley sedimentation at this time (Wakabayashi and Sawyer, 2001).

Considering that a deep crustal root was developed underneath the Sierra Nevada by 80 to 120 Ma, researchers have struggled to explain postulated Late Cenozoic uplift. Recent seismic studies clearly demonstrate that the southern Sierra Nevada presently lacks such a root and that the underlying mantle exhibits significant density contrasts (e.g. Wernicke *et al*., 1996; Ruppert *et al*., 1998). Xenoliths document the presence of a dense eclogite root underneath the crest of the Sierra Nevada in the Miocene (8–10 Ma), and its absence in the Pliocene (3·5 Ma), suggesting delamination

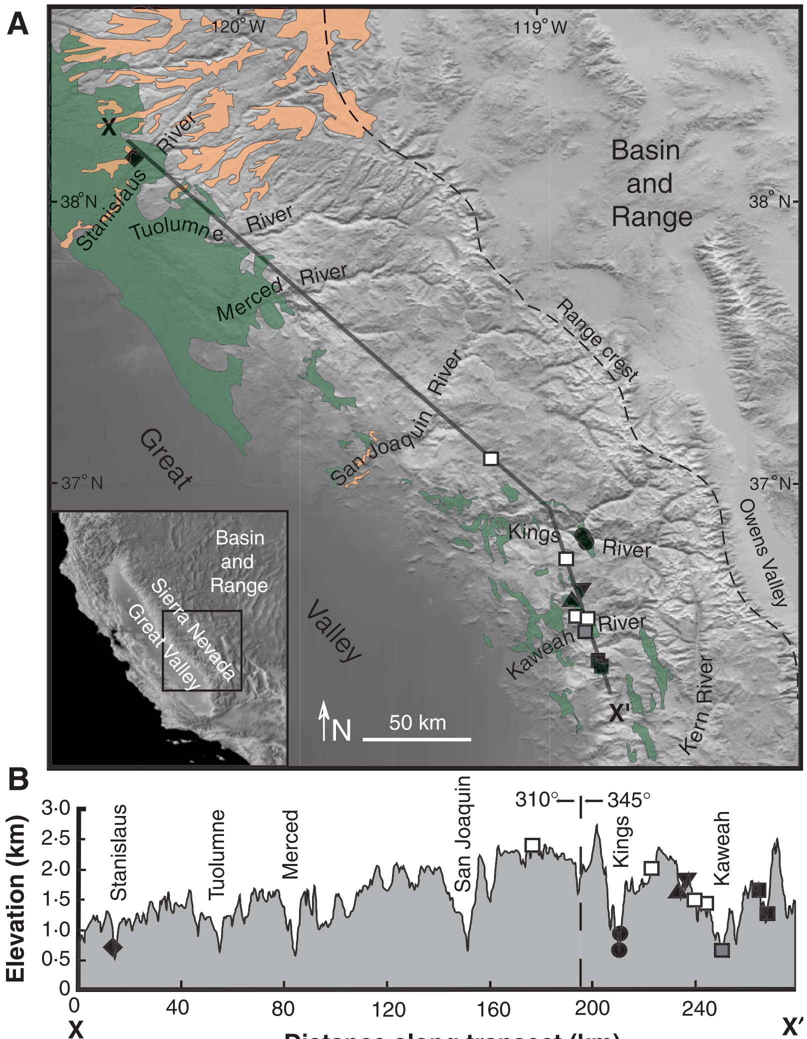

Figure 1. (A) Geologic and topographic setting of Sierra Nevada, showing locations of caves and interfluve surfaces sampled for cosmogenic nuclides. Highly fragmented Palaeozoic and Mesozoic metamorphic belt (dark grey; green in colour version online) containing cave-bearing marble bounds predominantly Cretaceous granitic rocks. Late Cenozoic volcanic deposits (white; orange in colour version online) blanket the northern Sierra, but are generally not present in southern Sierra. (B) Topographic profile along X–X′, showing systematic increase in mean altitude and local relief south of Stanislaus River, reaching maximum in vicinity of Kings River. See Figure 5 for symbol descriptions. This figure is available in colour online at www.interscience.wiley.com/journal/espl

occurred during this interval (Ducea and Saleeby, 1996, 1998; Saleeby *et al*., 2003). A pulse of volcanism in the southern Sierra at *c*. 3·5 Ma may mark the timing of delamination in this region (Manley *et al*., 2000; Farmer *et al*., 2002). Eclogite root delamination could drive ≥1 km of crestal uplift (Ducea and Saleeby, 1996; Jones *et al*., 2004), consistent with estimates based on tilted markers at the western edge of the range. An alternative uplift mechanism invokes late Cenozoic climate change. Small and Anderson (1995) called upon the flexural–isostatic response to accelerated erosion of the range in the late Cenozoic, suggesting that erosional unloading of the Sierra Nevada and simultaneous deposition of sediment in the adjacent Great Valley could explain roughly half to all of the observed tilt. In this scenario, relief production lowered the mean elevation of the range while summit elevations increased.

While the mechanism for late Cenozoic rock uplift is debated, the uplift itself is also questioned; (U-Th)/He apatite cooling ages apparently record considerable relief in the Sierra as early as the late Cretaceous (House *et al*., 1998, 2001). The observation that local relief (defined here as the vertical distance between canyon bottoms and adjacent canyon rims) was greater from *c*. 60 to 80 Ma than at present has been used to argue for a monotonic decline in mean

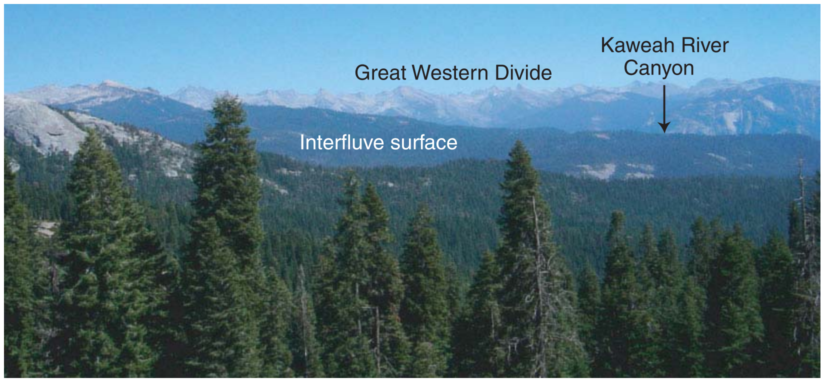

Figure 2. View southeast across low-relief, forested interfluve surfaces separating Kings and Kaweah river canyons. Kaweah River canyon is incised up to 1·8 km into interfluve surface. Distant peaks are part of Great Western Divide, a sub-range west of main range crest that reaches altitude of 4176 m. This figure is available in colour online at www.interscience.wiley.com/journal/espl

altitude and local relief during the Cenozoic. In this view, the range attained its maximum altitude and topographic relief in the late Mesozoic, and has been steadily decaying since, with no Cenozoic uplift (Wernicke *et al*., 1996; House *et al*., 1998). Oxygen isotopes in authigenic minerals east of the Sierra Nevada crest suggest a persistent rain shadow throughout the Miocene (Poage and Chamberlain, 2002), implying crestal altitudes were also high at that time. These isotopic data have been interpreted as indicating an apparently decreasing rain shadow since the Middle Miocene, which in turn has been interpreted as a loss of as much as 2 km of crestal altitude (Poage and Chamberlain, 2002).

One avenue for investigating rock uplift is by examining rates of river incision into bedrock, the principal erosional mechanism by which landscapes respond to regional tectonic forcing. Rock uplift steepens river gradients, and also increases river discharge by enhancing orographic precipitation; both serve to accelerate vertical bedrock incision relative to adjacent upland surfaces (Whipple and Tucker, 1999). In turn, river incision drives the evolution of mountainous topography by controlling the base level of erosion to which hillslopes respond (e.g. Burbank *et al*., 1996; Whipple *et al*., 1999). If the Sierra Nevada did in fact experience rock uplift in the past 5 Ma, then rivers draining the western slope ought to have accelerated their rate of incision in response, increasing topographic relief.

Rates of River Incision

Long-term river incision rates are typically measured by dating fluvial terraces (e.g. Burbank *et al*., 1996; Lave and Avouac, 2000; Reusser *et al*., 2004; Wolkowinsky and Granger, 2004), but can be difficult to constrain in mountain environments because rapidly incising rivers and frequent hillslope failure preclude formation of, or destroy, terraces. In the Sierra Nevada, previous estimates of river incision have been deduced from incision through dated volcanic remnants (Huber, 1981; Wakabayashi and Sawyer, 2001). However, these estimates suffer from five limitations: (1) widespread late Cenozoic volcanic deposits are not present in the southern half of the range (Figure 1A); (2) incision rates are mostly derived from a single dated surface, yielding time-averaged rates; (3) there is an indeterminate amount of time needed for rivers to incise through volcanic rocks before resuming basement bedrock incision (Wakabayashi and Sawyer, 2001); (4) remnant volcanic outcrops within canyons may not accurately depict the true canyon depth at the time of deposition; and (5) the ages of many volcanic units are not well constrained (e.g. the 5 to 33 Ma Mehrten Formation). Furthermore, volcanic deposits generally predate proposed uplift, so resulting time-averaged incision rates cannot capture the detailed erosional response to this event.

In their middle and lower reaches, many Sierra rivers flow through narrow marble gorges containing caves (Figure 3). These caves record river incision because they represent former river levels etched into bedrock. This is most clearly the case when rivers are briefly diverted into canyon walls, dissolving cave passages parallel to the river. Alternatively, tributary streams sink into fractured rock and dissolve caves along water table surfaces graded to river levels; changes in cave passage slope and morphology can be used to deduce palaeowater table gradients that precisely mark former river positions (Palmer, 1987, 1991). Subsequent bedrock incision lowers rivers relative to caves, leaving sediment-laden passages perched high in canyon walls. A vertical sequence of cave passages is therefore analogous to a flight of strath terraces, increasing with height above modern rivers and marking former river positions. In the Sierra, near-horizontal cave passages, originally formed at the water table, now occupy steep pinnacles and

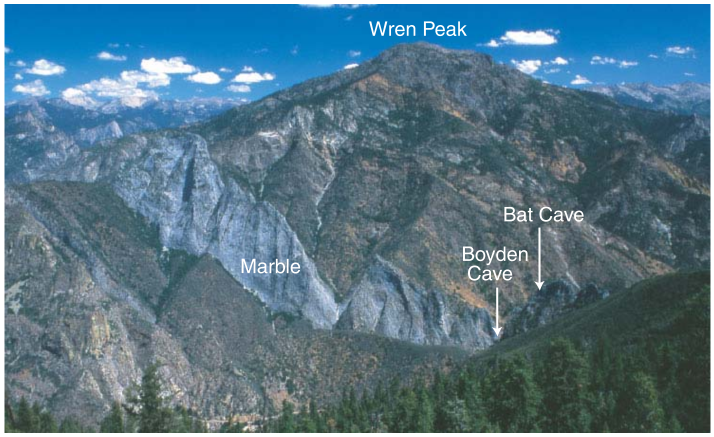

Figure 3. 2 km local relief of the South Fork Kings River canyon. Outcrop in centre left is vertically bedded cave-bearing marble of Boyden Cave metamorphic pendant. Range crest in far distance reaches altitude of 4342 m. Rivers headed in granitic rocks at range crest cut across marble unit, forming caves in canyon walls that are left perched above incising rivers. $^{26}Al/^{10}Be$ burial dating of granitic sediment washed into caves indicates development of 400 m inner gorge beginning *c.* 3 Ma. This figure is available in colour online at www.interscience.wiley.com/journal/espl

ridges far above present river levels (Figure 3). These passages are often cut across complex geologic structures, strengthening the argument that their development was fundamentally controlled by river position (Palmer, 1987). Presently active cave streams are graded to local base level, representing sound modern analogies for older caves in canyon walls.

Bedload sediment derived from granitic rocks upstream of caves is often transported through fluvially active cave passages. When incision lowers local base level, cave passages are abandoned by groundwater, sequestering sediment within. Shielded by bedrock, cave sediments can be preserved much longer than strath terraces, and in the Sierra are present where fluvial terraces are not. Most southern Sierra caves are preserved within the very steep walls of inner gorges; with few exceptions, higher (and therefore older) caves above inner gorges have been destroyed by hillslope retreat.

One of us (Stock) visited approximately 300 caves in the Sierra Nevada, and from these identified 18 caves with the following characteristics: (1) morphologies clearly linking them to former river positions; (2) they contained datable quartz-rich sediment of fluvial origin; and (3) they were positioned well downstream of glacial limits, where canyon cutting has been accomplished solely by river incision processes. These caves delineate a northwest-trending study transect across the central and southern Sierra, through the middle reaches of the major river canyons (Figure 1). Thus, the erosion rate and relief production arguments that follow apply strictly to the non-glaciated western slope of the range. Although Pleistocene glaciers significantly modified the topography of the High Sierra (>3500 m elevation), we argue that the topographic signature of late Cenozoic rock uplift, if present, lies in the river canyons.

Cosmogenic $^{26}Al/^{10}Be$ burial dating

We dated caves using cosmogenic $^{26}Al/^{10}Be$ burial dating of cave sediment (Granger *et al.*, 1997, 2001b; Granger and Muzikar, 2001; Partridge *et al.*, 2003). Aluminium-26 and ^{10}Be form in quartz-rich rocks near the Earth's surface, mostly by spallation reactions on O and Si, and to a much lesser extent by negative muon capture and fast muon interactions (Lal, 1991). *In situ* production of these nuclides decreases with depth below the surface. Production by nucleon spallation decreases roughly exponentially with a penetration length of 160 ± 10 g cm^{-2}, or roughly 60 cm in rock of density 2·6 g cm^{-3} (Masarik and Reedy, 1995). Production due to muon reactions is attenuated much less rapidly than spallogenic production, and therefore predominates at greater depth. Sediment accumulates ^{26}Al and ^{10}Be as it is eroded from hillslopes and transported down river networks (e.g. Brown *et al.*, 1995; Anderson *et al.*, 1996; Granger *et al.*, 1996). In a steadily eroding outcrop, the long-term concentration (N_i) of either ^{26}Al or ^{10}Be in quartz at the surface is determined by Equation 1 (Granger *et al.*, 2001a):

$$N_i = \frac{P_n}{(1/\tau_i + \rho\varepsilon/\Lambda_n)} + \frac{P_\mu}{(1/\tau_i + \rho\varepsilon/\Lambda_\mu)} \tag{1}$$

where P_n is the production rate by nucleon spallation, P_μ is the production rate by muons, τ_i is the radioactive meanlife ($\tau_{26} = 1{\cdot}02 \pm 0{\cdot}04$ My (Norris *et al*., 1983); $\tau_{10} = 2{\cdot}18 \pm 0{\cdot}09$ Ma (Middleton *et al*., 1993)), ρ is rock density (assumed $2{\cdot}7$ g cm^{-3}), ε is the rock erosion rate, Λ_n is the exponential penetration length for nucleons, and Λ_μ is the exponential penetration length for muons. The second term of Equation 1 may be separated into several terms of similar form to account for production at depth by stopped and fast muons (e.g. Granger *et al*., 2001a; Schaller *et al*., 2002; Heisinger *et al*., 2002a, b). The production rates of ^{26}Al and ^{10}Be vary with latitude, altitude and magnetic field variation (Lal, 1991; Stone, 2000) but the ratio of ^{26}Al and ^{10}Be production is fixed at 6·1 (Nishiizumi *et al*., 1989). If sediment is then washed deeply into a cave where it is shielded from subsequent cosmogenic ray exposure, nuclide production ceases and the concentrations of ^{26}Al and ^{10}Be decay according to:

$$N_i = (N_{i_0})e^{-t/\tau_i} \tag{2}$$

where t is the time since burial. Because ^{26}Al decays roughly twice as fast as ^{10}Be, the pre-burial ratio of these nuclides $(N_{26}/N_{10})_0$, decreases exponentially over time according to:

$$\frac{N_{26}}{N_{10}} = \left(\frac{N_{26}}{N_{10}}\right)_0 e^{-t(1/\tau_{26}-1/\tau_{10})} \tag{3}$$

where N_{26} and N_{10} are the concentrations of ^{26}Al and ^{10}Be and $(N_{26}/N_{10})_0$ represents the pre-burial ^{26}Al/^{10}Be ratio as determined from Equation 1. Equations 1 to 3 can be solved iteratively for converging solution of ε $(N_{26}/N_{10})_0$ and t (Granger *et al*., 1997). The ^{26}Al/^{10}Be ratio can be used to date buried sediment from *c*. 0·3 to 5 Ma (Granger and Muzikar, 2001).

Sierra Nevada caves present a nearly ideal setting for ^{26}Al/^{10}Be burial dating. Quartz-rich sediment slowly eroded from granitic basins is carried rapidly into caves. A lack of caves, alluvial terraces, and long-lived (≥100 ka) glacial moraines upstream of the sampled caves suggest that river sediment has not been shielded for long periods (> *c*. 300 ka) prior to burial in the caves. Once inside, tens to hundreds of metres of rock shield sediments such that post-burial nuclide production is negligible (Granger and Muzikar, 2001). The juxtaposition of marble caves downstream of granitic headwaters ensures that sampled sediment clearly originated from the surface.

We collected *c*. 300–500 g of granitic sediment from 18 cave sites, isolated ^{26}Al and ^{10}Be using standard techniques (Kohl and Nishiizumi, 1992; Granger *et al*., 2001b), and measured ^{26}Al/^{10}Be ratios by accelerator mass spectrometry at Lawrence Livermore National Laboratories. We solved for sediment burial ages and pre-burial erosion rates using Equations 1–3, and accounted for post-burial muogenic production following Partridge *et al*. (2003). As most samples are deeply buried (>30 m) in caves, the correction for post-burial production is negligible.

Cosmogenic burial ages and river incision rates

Cave sediment burial ages range from 0·32 ± 0·10 to ≥4·72 Ma (Table I, Figure 4), spanning the approximate age limits of the technique (Granger and Muzikar, 2001). Importantly, these ages also span the proposed rejuvenation of Sierra Nevada tectonism. Unburied sediments from modern rivers have ^{26}Al/^{10}Be ratios within error of the expected production ratio of 6·1 (Nishiizumi *et al*., 1989; Stone, 2000), suggesting that sediment does not enter caves with an inherited burial signal (Table I, Figure 4). Burial ages increase with height above modern river levels (Figure 5), as expected for the conceptual model of cave development outlined above. Replicate analyses indicate that cosmogenic burial ages reproduce within uncertainty, typically *c*. 0·08–0·2 Ma (see below). Due to a measured ^{26}Al/Al ratio at the limit of detection, buried sediment in Palmer Cave, the highest dated cave, provides only a minimum age of 4·72 Ma (Figures 3, 5); Palmer Cave may well be much older than this date implies.

Long-term river incision rates determined from dated caves (Table II) closely match previous estimates from volcanic deposits. Mean incision rates of *c*. 0·13 mm a^{-1} deduced from the oldest caves are strikingly similar to the mean incision rate of 0·15 mm a^{-1} from equivalent upstream positions of northern and central Sierra rivers (Wakabayashi and Sawyer, 2001). Furthermore, incision rates from the South Fork Kings River canyon of 0·15 mm a^{-1} averaged over 2·7 Ma (Bat Cave) and 0·12 mm a^{-1} averaged over 2·3 Ma (Morning Glory Cave) closely match an interpolated 5 Ma average rate of 0·13 mm a^{-1} from an equivalent upstream position in the adjacent San Joaquin River canyon (estimated from Huber, 1981). Close correspondence between cave- and volcanically derived incision rates suggests that caves accurately record river incision.

Although similar to earlier estimates, cave-derived incision rates provide additional detail not previously resolvable (Table II). Figure 5 suggests that incision rates have not been steady over the past 5 Ma, either in any one drainage, or for the western slope of the range as a whole. Rather, the caves suggest marked changes in incision rate through time.

Table I. Cosmogenic nuclide concentrations, burial ages, and pre-burial erosion rates from Sierra Nevada caves[a]

Sample	Location	River	P_{10}[b] (atom g^{-1})	^{26}Al[c] (10^4 atom g^{-1})	^{10}Be[c] (10^4 atom g^{-1})	^{26}Al/^{10}Be	Burial age (Ma)[d]	Pre-burial erosion (mm a^{-1})
CS-1	Crystal Stanislaus Cave	Middle Fork Stanislaus	18·0	26·56 ± 0·98	10·28 ± 0·21	2·59 ± 0·11	1·63 ± 0·08 (0·16)	0·046 ± 0·003 (0·010)
MG-1	Morning Glory Cave	Boulder Creek	14·4	23·09 ± 1·48	13·30 ± 0·33	1·79 ± 0·12	2·32 ± 0·19 (0·30)	0·021 ± 0·004 (0·010)
BAT	Bat Cave	South Fork Kings	36·5	11·30 ± 0·97	7·52 ± 0·56	1·50 ± 0·17	2·70 ± 0·21 (0·38)	0·079 ± 0·006 (0·016)
BOY-2	Boyden Cave	South Fork Kings	32·5	36·41 ± 1·36	12·43 ± 0·30	2·93 ± 0·13	1·38 ± 0·08 (0·15)	0·078 ± 0·005 (0·017)
BC-1	Bear Cave	South Fork Kings	32·5	56·24 ± 2·61	10·92 ± 0·28	5·15 ± 0·22	0·32 ± 0·10 (0·18)	0·163 ± 0·012 (0·035)
KGR-1	Modern river sediment	South Fork Kings	32·5	22·68 ± 1·17	3·62 ± 0·07	6·26 ± 0·35	−0·06 ± 0·11 (0·21)	0·508 ± 0·038 (0·108)
WR-1	Weis Raum Cave	Yucca Creek	16·5	9·46 ± 0·75	5·50 ± 0·12	1·72 ± 0·14	2·42 ± 0·16 (0·28)	0·055 ± 0·005 (0·012)
HCPL-2	Hurricane Crawl Cave	Yucca Creek	16·2	35·23 ± 1·93	9·44 ± 0·24	3·73 ± 0·23	0·93 ± 0·12 (0·24)	0·064 ± 0·005 (0·014)
CCBD	Bear Den Cave	Cascade Creek	18·7	97·53 ± 4·10	29·81 ± 0·70	3·27 ± 0·16	1·15 ± 0·09 (0·16)	0·031 ± 0·001 (0·005)
CCPR	Crystal Cave (Phosph. Room)	Cascade Creek	18·7	311·9 ± 8·7	91·8 ± 2·6	3·39 ± 0·14	1·00 ± 0·07 (0·14)	0·009 ± 0·0002 (0·001)
CCMH-1	Crystal Cave (Marble Hall)	Cascade Creek	18·5	79·17 ± 3·41	20·47 ± 0·49	3·87 ± 0·19	0·86 ± 0·09 (0·16)	0·035 ± 0·002 (0·007)
CCLR-1	Crystal Cave (Junction Room)	Cascade Creek	18·5	107·2 ± 3·5	23·79 ± 0·56	4·51 ± 0·18	0·56 ± 0·08 (0·15)	0·034 ± 0·003 (0·009)
KWH-1	Kaweah Cave	Middle Fork Kaweah	16·7	7·36 ± 0·78	1·49 ± 0·25	4·94 ± 0·99	0·40 ± 0·38 (0·85)	0·527 ± 0·039 (0·060)
KHR-1	Modern river sediment	Middle Fork Kaweah	22·0	35·25 ± 1·65	5·90 ± 0·16	5·90 ± 0·16	0·04 ± 0·10 (0·18)	0·202 ± 0·015 (0·043)
PLMR-1	Palmer Cave	South Fork Kaweah	18·5	≤1·21	2·34 ± 0·14	≤0·52	≥4·72	≤0·051
CL	Clough Cave	South Fork Kaweah	21·3	7·38 ± 0·48	2·09 ± 0·07	3·51 ± 0·25	1·03 ± 0·13 (0·28)	0·354 ± 0·026 (0·075)
NEW-1	New Cave	South Fork Kaweah	21·3	54·44 ± 2·44	13·85 ± 0·33	3·93 ± 0·20	0·83 ± 0·10 (0·18)	0·059 ± 0·004 (0·013)
LSRH-1	Soldiers Cave (Entrance Room)	South Fork Kaweah	18·9	50·24 ± 3·24	15·94 ± 0·38	3·15 ± 0·22	1·25 ± 0·13 (0·20)	0·038 ± 0·003 (0·008)
LSWR-1	Soldiers Cave (Waiting Room)	South Fork Kaweah	18·9	71·36 ± 2·97	19·63 ± 0·49	3·64 ± 0·18	0·98 ± 0·09 (0·17)	0·035 ± 0·002 (0·005)
LSLC-1	Soldiers Cave (Lower Corridor)	South Fork Kaweah	18·9	73·93 ± 3·21	15·03 ± 0·16	4·92 ± 0·24	0·40 ± 0·09 (0·17)	0·059 ± 0·004 (0·010)

[a] Some of these data were originally reported in Stock *et al*. (2004).

[b] Basin mean ^{10}Be production rate from basin hypsometry upstream of caves; multiply by 6·1 to get mean ^{26}Al production rate (Nishiizumi *et al*., 1989; Stone, 2000). Production rates scaled for altitude and latitude following Stone (2000) for neutrons and Granger *et al.* (2001a) for muons, assuming sea-level high latitude (SLHL) production rates of $P_{26} = 31·1$ atom g^{-1} a^{-1} and $P_{10} = 5·1$ atom g^{-1} a^{-1}, (Stone, 2000), and SLHL stopped muogenic production rates of $P_{26} = 0·80$ atom g^{-1} a^{-1}, and $P_{10} = 0·10$ atom g^{-1} a^{-1} (Heisinger *et al*., 2002b).

[c] Measured ^{26}Al/Al and ^{10}Be/Be ratios were normalized to ICN ^{10}Be and NBS ^{26}Al standards prepared by K. Nishiizumi. Measured ratios were converted to atom g^{-1} using the amount of Be carrier added and by measuring stable Al measurements on an ICP-OES. Stable Al measurements were assigned 4 per cent error.

[d] Burial ages calculated using Equations 1–3. Uncertainties represent 1σ measurement uncertainty, with systematic uncertainties in production rates, attenuation coefficients, ^{26}Al/^{10}Be production ratio, and decay constants (Norris *et al*., 1983; Middleton *et al*., 1993) added in quadrature and shown in parentheses. We report burial ages based on the commonly accepted ICN ^{10}Be standard, and a ^{10}Be meanlife of 2·18 ± 0·09 My. Some researchers (e.g. Partridge *et al*., 2003) have adopted an alternative NIST ^{10}Be standard, and a meanlife of 1·93 ± 0·10, which would increase our reported burial ages; for example, the age for Bat Cave based on the NIST standard is 2·90 ± 0·21 (0·49).

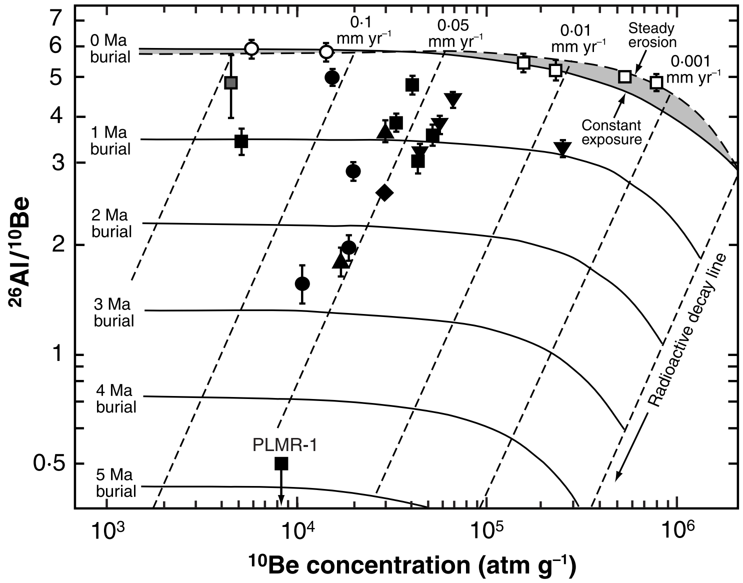

Figure 4. Cosmogenic nuclide data from buried cave sediments and surface bedrock samples, plotted logarithmically as $^{26}Al/^{10}Be$ versus ^{10}Be concentration. ^{10}Be concentrations normalized for local production rate, assuming sea-level, high-latitude ^{10}Be production rate of 5·1 atom g^{-1} a^{-1} (Stone, 2000). Samples with simple history of exposure and steady erosion plot within shaded area between constant exposure and steady erosion lines (Lal, 1991; Granger and Muzikar, 2001). Once buried, $^{26}Al/^{10}Be$ in sediment decreases exponentially, parallel to dashed radioactive decay line. Burial isochrons shown at million year intervals. Open circles, unburied river sediment; open squares, surface bedrock samples. See Figure 5 for other symbol descriptions. Error bars represent 1σ analytical uncertainty.

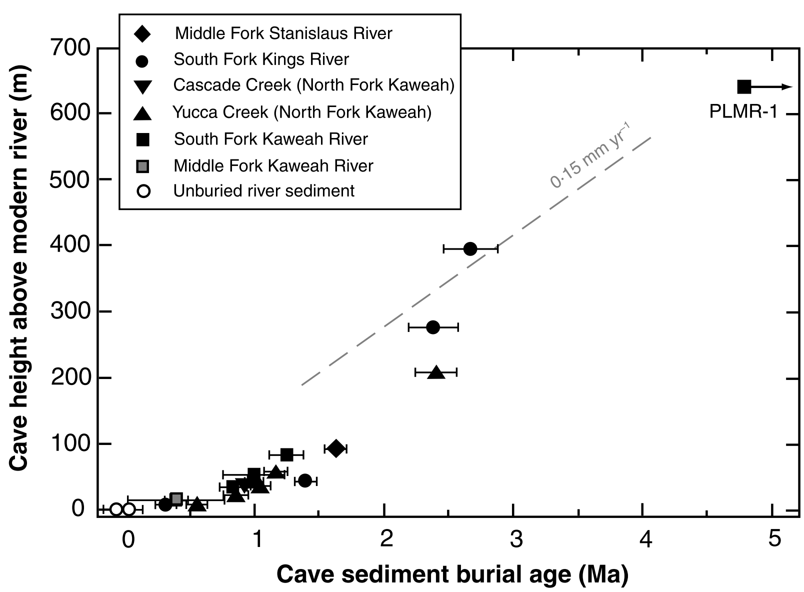

Figure 5. Five-million-year incision history for central and southern Sierra Nevada rivers determined by cosmogenic $^{26}Al/^{10}Be$ burial dating of cave sediments. Unburied river sediments (shown as open symbols) yield burial ages indistinguishable from zero, suggesting no inherited burial signal in cave sediments. Dashed line denotes average range-wide incision rate based on incision through *c.* 5 Ma uppermost Mehrten Formation (Wakabayashi and Sawyer, 2001). Sample PLMR-1 yields a minimum age of 4·72 Ma. Caves show a pulse of rapid incision from *c.* 3 to 1·5 Ma (shaded area), followed by much slower incision, a change evident across the study transect. Error bars represent 1σ analytical uncertainty.

Table II. River incision rates from Sierra Nevada caves

Sample	Location	River	Cave height[a] (m)	Burial age (Ma)	River incision[b] (mm a^{-1})
CS-1	Crystal Stanislaus Cave	Middle Fork Stanislaus	90 ± 5 (92)	1·63 ± 0·08	0·06 ± 0·01
MG-1	Morning Glory Cave	Boulder Creek	274 ± 5	2·32 ± 0·19	0·12 ± 0·01
BAT	Bat Cave	South Fork Kings	395 ± 2	2·70 ± 0·21	0·27 ± 0·04
BOY-2	Boyden Cave	South Fork Kings	42·5 ± 1	1·38 ± 0·08	0·03 ± 0·01
BC-1	Bear Cave	South Fork Kings	8 ± 1	0·32 ± 0·10	0·02 ± 0·01
WR-1	Weis Raum Cave	Yucca Creek	212 ± 2	2·42 ± 0·16	0·12 ± 0·02
HCPL-2	Hurricane Crawl Cave	Yucca Creek	36 ± 3 (39·5)	0·93 ± 0·12	0·04 ± 0·01
CCBD	Bear Den Cave	Cascade Creek	58 ± 1	1·15 ± 0·09	0·14 ± 0·08
CCPR	Crystal Cave (Phosph. Room)	Cascade Creek	36·5 ± 1	1·00 ± 0·07	0·10 ± 0·06
CCMH-1	Crystal Cave (Marble Hall)	Cascade Creek	22·5 ± 1	0·86 ± 0·09	0·05 ± 0·02
CCLR-1	Crystal Cave (Junction Room)	Cascade Creek	8·5 ± 1	0·56 ± 0·08	0·02 ± 0·01
KWH-1	Kaweah Cave	Middle Fork Kaweah	15 ± 1	0·40 ± 0·38	0·04 ± 0·04
PLMR-1	Palmer Cave	South Fork Kaweah	645 ± 10	≥4·72	≤0·16
LSRH-1	Soldiers Cave (Entrance Room)	South Fork Kaweah	84 ± 2	1·25 ± 0·13	0·14 ± 0·09
CL	Clough Cave	South Fork Kaweah	53·5 ± 2	1·03 ± 0·13	0·31 ± 0·70
LSWR-1	Soldiers Cave (Waiting Room)	South Fork Kaweah	38 ± 4 (41)	0·98 ± 0·09	–
NEW-1	New Cave	South Fork Kaweah	34 ± 2	0·83 ± 0·10	0·06 ± 0·02
LSLC-1	Soldiers Cave (Lower Corridor)	South Fork Kaweah	10 ± 3 (12·5)	0·40 ± 0·09	0·03 ± 0·01

[a] Cave height above local base level river based on inferred palaeowater table gradients; where different, absolute heights are shown in parentheses. Height error combines survey error and palaeowater table gradient uncertainty.

[b] For tiered caves, incision rates are calculated using the distance between cave passages (see Figures 6–9); for example, the distance between palaeowater table levels inferred from Weis Raum and Hurricane Crawl caves (176 m) yields an incision rate of 0·12 ± 0·02 mm a^{-1} for the period 2·42 to 0·93 Ma.

For example, the South Fork Kings River incised at 0·27 mm a^{-1} from 2·7 to 1·4 Ma but slowed markedly to *c*. 0·02 mm a^{-1} after 1·4 Ma (Figure 6). Similarly, multiple dated cave levels in the South Fork Kaweah River canyon document incision peaking at *c*. 1 Ma at 0·35 mm a^{-1}, slowing thereafter to rates of 0·05–0·03 mm a^{-1} (Figure 7). In Yucca Creek canyon, a tributary of the North Fork Kaweah River, an incision rate of 0·12 mm a^{-1} from 2·4 to 0·9 Ma slowed to 0·04 mm a^{-1} after 0·9 Ma (Figure 8). Nearby Cascade Creek also shows a decrease in incision from 0·18 to 0·02 mm a^{-1} over the past 1·2 Ma. In all of the southern Sierra canyons studied, caves younger than 1 Ma consistently yield low incision rates of 0·02 to 0·05 mm a^{-1} (Table II, Figure 5).

Further north in the Stanislaus River canyon, a cave-derived incision history overlaps with that derived from the 9·2 Ma Table Mountain Latite (TML) erupted near the crest of the range and emplaced within the ancestral Stanislaus River canyon. Following deposition of the TML, the Stanislaus River has incised some 550 m, most of which is within a narrow gorge (Figure 9). Crystal Stanislaus Cave indicates that inner gorge incision was well underway prior to 1·6 Ma. Although the record here suggests little change in incision rate since 9·2 Ma (Figure 9), it is determined by only two points, leading to substantial time-averaging; a similar temporal pattern of incision as that shown by caves further south is certainly plausible at this location. Thus, cave-derived incision rates consistently show a pulse of incision that began in the Late Pliocene and had decreased considerably by 1·5 Ma. That this pattern is documented across much of the range suggests that rivers are responding to a range-wide perturbation.

Onset of renewed incision and inner gorge formation

Because few caves containing datable sediment exist outside of the inner gorges, our data do not clearly show when the most recent phase of accelerated incision began at the cave sites, only that it was underway by 2·7 Ma. However, the minimum age of 4·72 Ma for Palmer Cave, the one dated cave located above the inner gorges (Figure 7), does suggest a maximum early Pliocene incision rate of 0·07 mm a^{-1} (Figure 5); if Palmer Cave is in fact much older than 4·72 Ma, then early Pliocene incision was much slower than 0·07 mm a^{-1}. Thus, the most recent phase of accelerated incision appears to have begun in Late Pliocene time.

Landscape morphology suggests that the switch to more rapid incision occurred midway up river profiles rather abruptly at *c*. 3 Ma. Most southern Sierra Nevada river canyons display a prominent two-tiered structure, with narrow inner gorges set within deeper and wider canyons (Figures 6–9; Matthes, 1960; Bateman and Wahrhaftig, 1966),

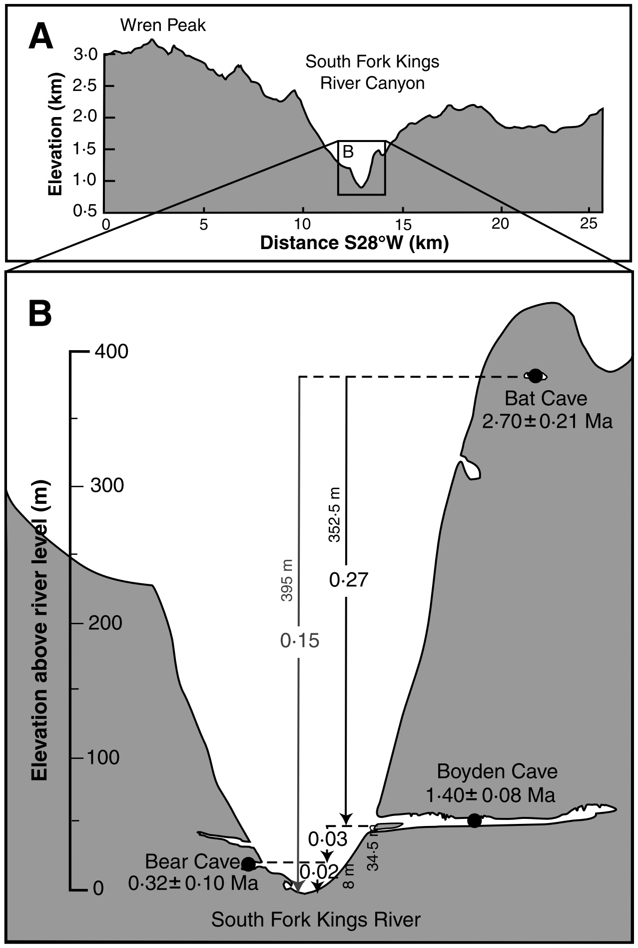

Figure 6. Dated caves and incision rates in South Fork Kings River canyon. (A) Topographic profile across South Fork Kings River canyon showing *c.* 2 km local relief. (B) Inner gorge containing multiple dated caves. Long-term rate of incision based on oldest dated cave (2·7 Ma Bat Cave) of 0·15 mm a^{-1} matches well rates derived from incision through 5 Ma volcanic flows (Wakabayashi and Sawyer, 2001). However, younger caves reveal fast incision before 1·4 Ma followed by an order of magnitude decline in incision rate after. Although caves demonstrate 395 m of canyon incision since 2·7 Ma, larger context shown in (A) illustrates that this represents only *c.* 20 per cent of present local relief.

suggesting a two-phase erosional history. Inner gorge structures generally indicate rapid incision following a prolonged period of stable base level of erosion (Bull, 1991). Although large tributary streams with high stream power enter inner gorges at grade, smaller tributaries with lower stream power are perched above modern rivers, marking the river position before inner gorge development. In their middle reaches, tributary streams entering southern Sierra river canyons typically exhibit smooth concave profiles below upland surfaces, as expected for graded streams at their base level of erosion (Bull, 1991). In contrast, the lower reaches display prominent convexities as they drop steeply into inner gorges. The heights at which tributaries 'hang' above modern rivers vary depending on their upstream position along river profiles, but are generally between 350 and 500 m. Note that these are not hanging valleys formed by glacial erosion, as these tributaries are well downstream of the maximum glacial extent. Tributaries in the San Joaquin River canyon descend from upland surfaces into broad, low-gradient canyons before cascading some 450–480 m into the inner gorge of that canyon (Matthes, 1960). Although Matthes posited a Pleistocene age for this inner gorge (corresponding to his Canyon stage of erosion), the onset of incision has, until now, been essentially unconstrained. However, at the cave site in the South Fork Kings River canyon, tributaries exhibiting concave middle profiles 'hang' above the modern river *c.* 350–400 m (Figure 10). This is similar to the height of Bat Cave (395 m), suggesting that the 2·7 ± 0·2 Ma age for Bat Cave marks the onset of more rapid incision at this point midway up the river profile. In

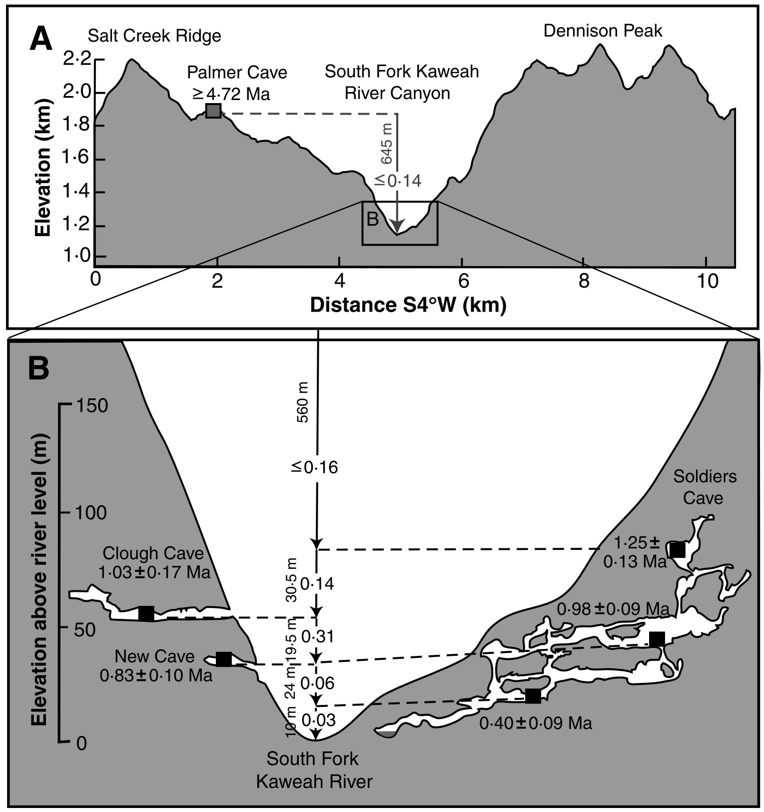

Figure 7. Dated caves and incision rates in the South Fork Kaweah River canyon. (A) Topographic profile across South Fork Kaweah River canyon showing *c.* 1 km local relief. Buried sediments in Palmer Cave yield a minimum age of 4·72 Ma and thus a maximum long-term incision rate of 0·14 mm a^{-1}; this rate is also a maximum because no palaeowater table gradient is inferred. (B) Inner gorge containing multiple dated cave levels. Inferred palaeowater table gradients shown as dashed lines. Distance between dated intervals indicates a pulse of incision peaking at 0·35 mm a^{-1} before 1 Ma and falling to 0·03 mm a^{-1} after 0·4 Ma. Note that the palaeowater table gradient inferred from the Waiting Room of Soldiers Cave projects to the level of New Cave; the 0·83 Ma age of New Cave is used to calculate the incision rate because it is closer to the river and is a therefore more precise marker of former river level.

this and other canyons, younger caves demonstrate that inner gorges were deeply incised by 1 Ma (Figures 6–9). We hypothesize that initial canyon incision was followed by a prolonged period of stable local base level, during which time tributary streams became graded. Renewed incision at the cave sites beginning at 3 Ma swiftly lowered local base level by 300–400 m, an event to which all but the largest tributaries are still responding. Slow propagation of the erosional pulse into adjacent uplands has helped to maintain the broad interfluve surfaces (Figure 2).

Pre-burial erosion rates

In addition to burial ages, iterative solution of Equations 1–3 yields nuclide concentrations in sediment prior to burial (Table I, Figure 4). These may be interpreted either in terms of the rate of basin erosion or as the duration of sediment transport and/or storage in the fluvial system (e.g. Anderson *et al*., 1996; Granger *et al*., 1996; Schaller *et al*., 2001). We interpret pre-burial concentrations as basin erosion rates because sediment transport is likely rapid in the steep catchments upstream of the sampled caves.

Pre-burial erosion rates range widely from 0·007 to 0·35 mm a^{-1} (Table I, Figure 4). Although this variation may reflect real erosion rate variations due to different surface processes acting in basins of varying size, we suspect that it is at least partially influenced by our sampling. Nuclide concentrations in numerous sand grains record basin-averaged erosion rates because the grains are assumed to derive uniformly from across the basin. However, because the origin of sand in caves may be ambiguous, and because coarse clasts clearly indicate bedload transport and are unlikely to be

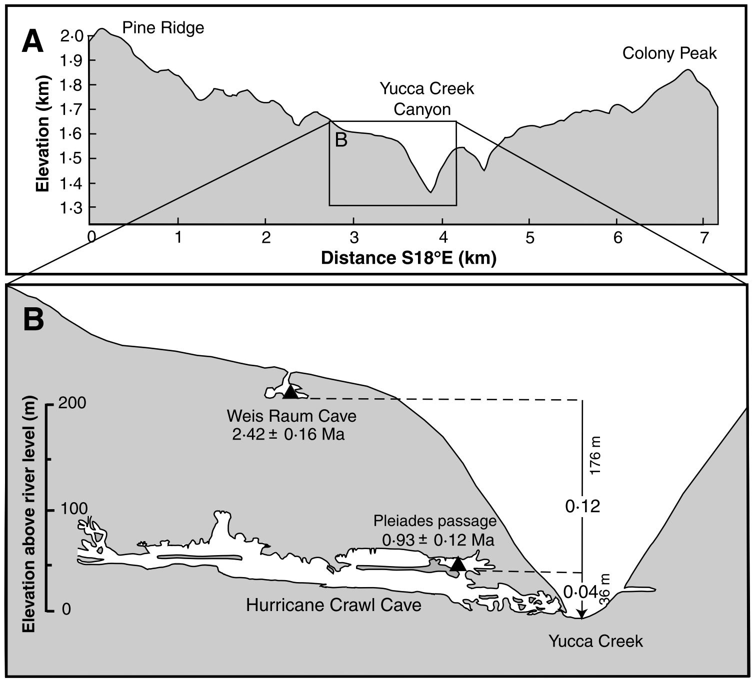

Figure 8. Dated caves and incision rates in Yucca Creek canyon. (A) Topographic profile across Yucca Creek canyon showing *c.* 750 m local relief. (B) Inner gorge showing position of Weis Raum and Hurricane Crawl caves. Inferred palaeowater table gradients shown as dashed lines. Sediment burial dates reveal relatively fast incision of 0·12 mm a^{-1} from 2·4 to 0·9 Ma, followed by slower incision of 0·04 mm a^{-1} from 0·9 Ma to present.

remobilized, we sampled single cobbles or coarse gravel (typically <30 clasts) for burial dating. While this strategy helps to ensure accurate cave ages, it limits the usefulness of pre-burial nuclide concentrations, as single clasts may not estimate well the average basin erosion rate. To test this, we chose two caves originally dated by a single clast, created replicate samples by amalgamating additional clasts from the same deposits, and then processed as above. Replicate samples yielded burial ages identical within analytical error to the original samples, but in both cases incorporating additional clasts increased pre-burial rates of erosion (Table III). Although the number of clasts analysed in the replicate samples do not provide statistically robust mean erosion rates (Anderson *et al*., 1996), these preliminary results do suggest a reduction in basin erosion after 1·2 Ma, consistent with the overall trend established by the burial ages. Future work utilizing >30 clasts will better constrain both burial ages and pre-burial erosion rates.

Additional uncertainty in pre-burial erosion rates results from the fact that most of the studied caves draw sediment from large catchments with hundreds to thousands of metres of relief, and we have no independent knowledge of where within these basins the few clasts we analysed originated. Most studies use the modern basin hypsometry to calculate a mean production rate for each catchment (e.g. Schaller *et al*., 2002). While we have employed this method (Table I), taking into account relief changes indicated by the older caves (see below), we acknowledge the additional uncertainty in pre-burial erosion rates introduced by potentially large changes in basin hypsometry, and perhaps mean altitude, since deposition of the older cave sediments.

Despite these uncertainties, Figure 4 shows that the majority of pre-burial erosion rates fall between 0·01 and 0·1 mm a^{-1}, with a mean ± s.e. of 0·09 ± 0·002 mm a^{-1}. This indicates that, as expected, cave sediments derive from hillslopes eroding at rates bracketed by relatively fast canyon incision (up to 0·3 mm a^{-1}) and much slower upland erosion (*c.* 0·01 mm a^{-1}; see below).

Estimates of Palaeorelief

The positions of dated caves in the landscape provide estimates of local palaeorelief, i.e. the amount of local relief present when the caves formed (Table IV). For example, the depth of the South Fork Kings Canyon prior to 2·7 Ma was at least 1600 m, the distance from the highest dated cave (Bat Cave) to the adjacent north rim of the canyon near

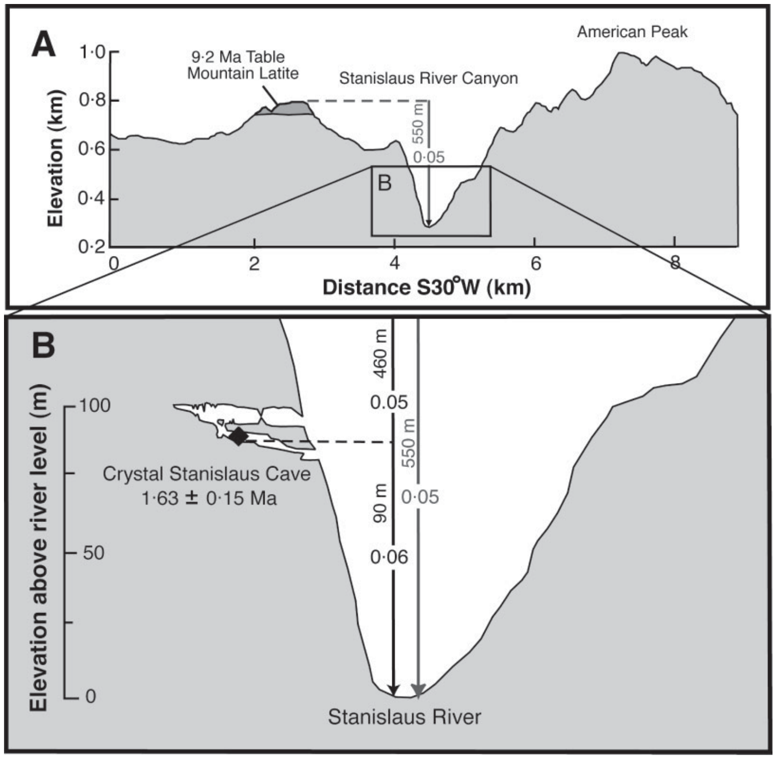

Figure 9. Dated caves and incision rates in the Stanislaus River canyon. (A) Topographic profile across Stanislaus River canyon showing *c.* 750 m local relief. Table Mountain Latite (TML) erupted near Sierra Nevada crest and flowed down ancestral Stanislaus River canyon *c.* 9·2 Ma (Dalrymple, 1964), preserving river position at that time. Topographic inversion has left TML as a meandering tableland; subsequent river incision cut *c.* 400 m deep inner gorge. Depth of river below TML yields 9·2 Ma average incision rate of 0·05 mm a^{-1}, a minimum estimate as no initial canyon relief is assumed. (B) Crystal Stanislaus Cave, 1·6 Ma old, located well within inner gorge, yields incision rate of 0·05 mm a^{-1} from 9·2 to 1·6 Ma, and 0·06 mm a^{-1} thereafter.

Table III. Dependence of sample size on pre-burial erosion rates

Cave	Sample	n[a]	Burial age (Ma)	Pre-burial erosion rate (mm a^{-1})	Difference[b] (%)
Crystal	CCBD-1	1	1·16 ± 0·09	0·021 ± 0·001	64·5
(Bear Den)	CCBD-2	12	1·14 ± 0·09	0·040 ± 0·003	
Crystal	CCPR-1	1	1·06 ± 0·07	0·007 ± 0·004	35·3
(Phosphorescent)	CCPR-2	8	0·94 ± 0·07	0·010 ± 0·007	

[a] Number of sediment clasts in sample.
[b] Percentage difference of amalgamated sample from original single clast sample.

Wren Peak (Figures 3, 6A). Caves in other drainages also show substantial (400–1100 m) local palaeorelief (Table IV, Figures 7A–9A). These estimates are minima because they assume no lowering of rim elevations since caves formed.

Considerable (1–1·5 km) pre-Pliocene relief in the southern Sierra agrees well with independent observations. For example, the Tuolumne River canyon (Figure 1) contains late Cenozoic deposits inset hundreds of metres below basement bedrock ridges. Reconstruction of the 10 Ma San Joaquin River channel suggests ≥1000 m of palaeorelief in parts of that canyon (Huber, 1981; Wakabayashi and Sawyer, 2001). Dated volcanic flows in the upper San Joaquin River region indicate that, prior to 3·5 Ma, canyons were at least 150 m deep and nearly 1500 m of relief was present near the range crest (Dalrymple, 1964). Canyons in the Kern River region were at least 240 m deep *c.* 3·5 Ma, while relief near the crest was *c.* 1400 m (Dalrymple, 1963). Palaeorelief increases from north to south (Wakabayashi and Sawyer, 2001),

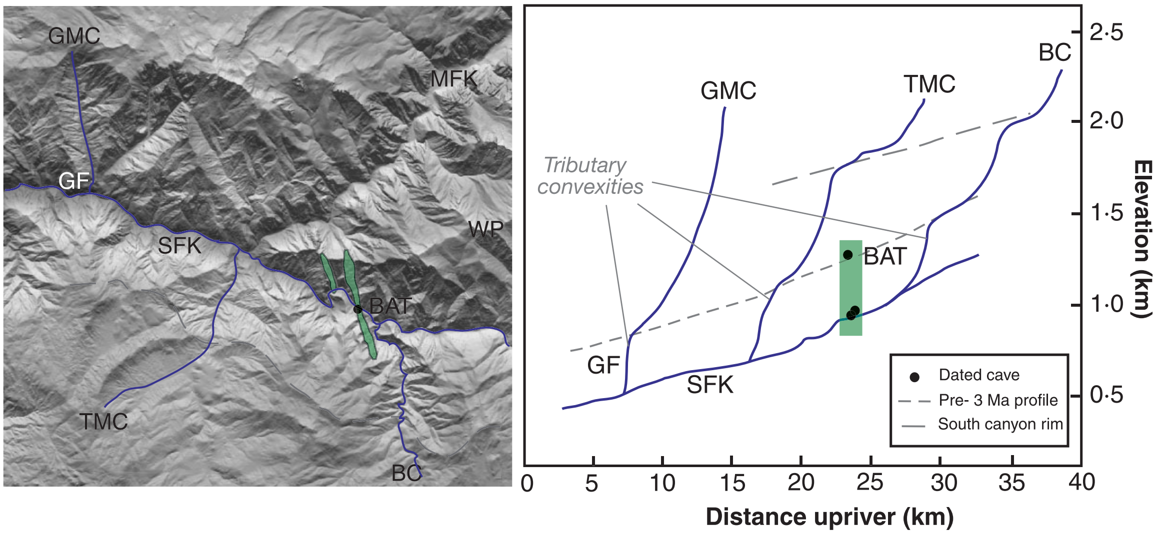

Figure 10. Longitudinal profiles of tributary streams entering South Fork Kings River canyon. Tributary streams show prominent convex steps in otherwise concave profiles as they cascade steeply into inner gorge. Tributary convexities 'hang' *c.* 350–400 m above river, similar to height of 2·7 Ma Bat Cave, suggesting a prolonged period of stable base level followed by rapid incision beginning *c.* 3 Ma. Marble belt shown in dark grey (green in colour version online). BAT, Bat Cave; BC, Boulder Creek; GF, Garlic Falls; GMC, Garlic Meadow Creek; MFK, Middle Fork Kings River; SFK, South Fork Kings River; TMC, Tenmile Creek. This figure is available in colour online at www.interscience.wiley.com/journal/espl

Table IV. Estimates of Sierra Nevada local palaeorelief

River	Cave	Burial age (Ma)	Modern local relief[a] (m)	Local palaeorelief[b] (m)
Stanislaus	Crystal Stanislaus	1·63 ± 0·08	700	600
Boulder Creek	Morning Glory	2·34 ± 0·19	1850	1580
South Fork Kings	Bat	2·70 ± 0·21	2000	1600
Cascade Creek	Bear Den	1·17 ± 0·09	480	420
Yucca Creek	Weis Raum	2·42 ± 0·16	610	400
Middle Fork Kaweah	Kaweah	0·40 ± 0·38	1390	1350
South Fork Kaweah	Palmer	≥4·72	1450	≥750
South Fork Kaweah	Clough	1·25 ± 0·13	1450	1360

[a] Present local relief is the maximum distance from canyon bottom to adjacent canyon rim within 5 km of cave sites.

[b] Local palaeorelief is distance from highest dated cave to adjacent canyon rim within 5 km of cave sites. Palaeorelief estimates are minima because they assume no lowering of rim altitudes.

coinciding with a similar increase in modern relief along the study transect (Figure 1B). In the north, the narrow inner gorges represent the majority of canyon depth, while in the south they are set into the bottoms of broad, deep canyons.

If the most recent episode of rock uplift commenced *c.* 3·5–5 Ma, as many researchers suggest (Unruh, 1991; Manley *et al.*, 2000; Wakabayashi and Sawyer, 2001; Jones *et al.*, 2004), then up to 2 km of incision at very rapid rates (2 mm a^{-1}) before 3·5 Ma must be invoked to produce all of the present local relief. Tributary stream profiles do not suggest such rapid incision, nor does the minimum age of 4·72 Ma for Palmer Cave (Figure 5). Sustained rapid incision throughout the Pliocene is therefore unlikely, signifying that the southern Sierra was already an elevated, moderately high relief landscape prior to renewed uplift (Wakabayashi and Sawyer, 2001) and maintained altitudes sufficient to cast a significant rain shadow since at least the Miocene (Poage and Chamberlain, 2002). In fact, much of the present topography in the southern Sierra could be relict from a pre-Eocene episode of uplift, possibly even from the Late Cretaceous (Wakabayashi and Sawyer, 2001). Although the early history of incision remains unclear, inset caves and volcanic deposits indicate at least a two-phase incision history with the most recent phase beginning *c.* 3 Ma.

Upland Erosion Rates and Relief Production

Many of the arguments for and against late Cenozoic uplift depend on whether topographic relief increased or decreased. For example, the flexural–isostatic rock uplift mechanism requires an increase in relief (Small and Anderson, 1995, 1998; Molnar and England, 1990). However, based on apatite (U-Th)/He thermochronometry, House *et al*. (1998) posited that high local relief *c*. 60–80 Ma decreased monotonically since that time; by inference, crestal elevations also decreased, and no late Cenozoic uplift is called for. Poage and Chamberlain (2002) also suggest a late Cenozoic decrease in crestal elevation; because relief production would drive at least some flexural–isostatic uplift of summits, the crestal elevation loss scenario advocated by Poage and Chamberlain (2002) also requires a loss of relief.

Any decrease in relief demands that erosion of upland (interfluve and summit) surfaces outpaces river incision. Thus, quantitative constraints on both canyon and upland erosion are needed to test for relief production. Caves dated by ^{26}Al/^{10}Be provide rates of canyon deepening. To determine rates of erosion on the immediately adjacent upland surfaces, we measured concentrations of ^{26}Al and ^{10}Be in granitic rocks exposed on these surfaces. Because the cosmic ray flux that produces cosmogenic nuclides decreases exponentially with depth below the Earth's surface, accumulated ^{26}Al and ^{10}Be concentrations in the top few centimetres of bare bedrock surfaces record the long-term erosion rates of these surfaces (e.g. Lal, 1991; Small *et al*., 1997; Granger *et al*., 2001a; Bierman and Caffee, 2002).

We sampled four interfluve surfaces along the study transect separating the major river canyons (Figure 1). Most interfluve surfaces are composed of low-relief upland topography with minimal shielding (Figures 2, 11). Sample sites are located several kilometres from incised river canyons (Figure 1), and were not glaciated during the late Pleistocene or Holocene (Matthes, 1960, 1965). We collected *c*. 100 g of granitic rock from each site, typically as thin (1–3 cm) exfoliation slabs, and measured their ^{26}Al and ^{10}Be concentrations as above. We used Equation 1 to calculate erosion rates, determining the contribution of muons following Granger *et al*. (2001a), though we note that for slowly eroding

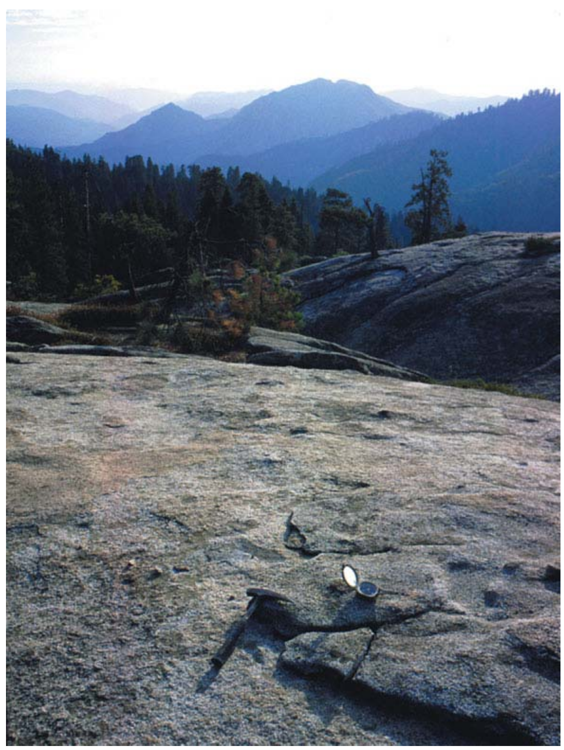

Figure 11. Beetle Rock, a granitic dome on interfluve surface separating Kaweah River canyons. Bare bedrock interfluve surfaces along study transect were not glaciated during Pleistocene; lack of regolith cover suggests erosion is limited by efficiency of weathering processes. Concentrations of ^{26}Al and ^{10}Be yield an erosion rate of 0·003 mm a^{-1}averaged over *c*. 145 ka for this surface; such low rates of erosion typify upland surfaces. Rock hammer and compass for scale. This figure is available in colour online at www.interscience.wiley.com/journal/espl

surfaces the contribution of muons is low because radioactive decay has reduced the fraction of nuclides produced by muons at depth.

Aluminium-26 and ^{10}Be concentrations from sampled bedrock surfaces plot within 1σ of the model curves for steady erosion or constant exposure (Figure 4), suggesting no extended burial of interfluve surfaces. Consequently, nuclide concentrations are interpreted to reflect bedrock erosion rates ranging from 0·003 to 0·019 mm a^{-1} (Table V). Erosion rates are averaged over a characteristic erosional timescale of $\Lambda\rho^{-1}\varepsilon^{-1}$, the time required to erode a layer of rock *c*. 60 cm thick; erosional timescales for bedrock samples range from 160 to 30 ka (Table V). These values yield a mean erosion rate for Sierra Nevada interfluve surfaces of 0·010 ± 0·001 mm a^{-1} averaged over 86·5 ± 6·4 ka (mean ± s.e.). Such slow rates are comparable to those measured immediately east of the crest in the northern (mean 0·011 mm a^{-1}; Granger *et al*., 2001a) and southern (0·003 mm a^{-1}, Small *et al*., 1997) Sierra Nevada, in the adjacent Owens Valley (0·007 mm a^{-1}; Bierman, 1994), and in other North American granitic alpine environments (mean 0·007 mm a^{-1}; Small *et al*., 1997) over equivalent timescales.

That many upland surfaces are bare bedrock indicates that erosion is not limited by transport of regolith. Rather, erosion is apparently limited by the rate at which bedrock is weathered (Small *et al*., 1997). We posit that the weathering-limited erosion rates of upland surfaces were roughly steady over the past few million years. Our basis for this assumption is threefold. First, interfluve sample sites are far from adjacent canyons, so that their rates of erosion have been effectively isolated from inner gorge incision (e.g. Small and Anderson, 1998; Riebe *et al*., 2000; Anderson, 2002). Temporal changes in interfluve erosion rates must therefore be driven by changes in the weathering climate. However, climatic effects appear to exert minimal control on erosion rates of non-glaciated granitic surfaces in the Sierra Nevada (Riebe *et al*., 2001). Furthermore, because two of the erosion rate measurements are averaged over ≥100 ka, they encompass erosion rate variations over a full glacial–interglacial cycle. As such, these low rates are likely representative of rates over at least the Quaternary. Finally, preservation of 3·5 to 12 Ma volcanic flows on the broad Kings and San Joaquin interfluves suggest that these surfaces have not been deeply eroded in the past few million years (Jones *et al*., 2004).

If this reasoning is correct, a long-term picture of relief production emerges. Although the Great Valley sedimentation history, and palaeotopgraphy implied by (U-Th)/He thermochronometry suggests rapid incision and relief production during the Cretaceous (House *et al*., 1998), by Oligocene time river incision rates in the northern Sierra were extremely low at *c*. 0·003 mm a^{-1} (Wakabayashi and Sawyer, 2001). If uplands were contemporaneously eroding three to four times faster, at *c*. 0·01 mm a^{-1}, then local relief should have decreased between the Eocene and Pliocene by *c*. 500 m. A sharp increase in river incision rates to *c*. 0·3 mm a^{-1} from *c*. 3 to 1·5 Ma outpaced upland erosion by more than an order of magnitude, rejuvenating relief by incising inner gorges. Since 1·5 Ma, local relief has increased more slowly, as incision outpaced interfluve erosion by only factors of two to four. Thus, although relief may have diminished throughout much of the Cenozoic, relief production has dominated since the Late Pliocene and continues today.

Our data do not support the notion that relief has decreased monotonically throughout the Cenozoic, although they do allow an extended period of relief reduction prior to the Late Pliocene (House *et al*., 1998). Because relief production likely incited rock uplift through flexural–isostatic compensation (Molnar and England, 1990; Small and Anderson, 1995), and because rock uplift at the crest likely outpaced local weathering rates there, the altitude of the Sierra crest has probably increased over the past few million years. This runs counter to the proposed loss of crestal altitude during this time inferred from stable isotopes in weathering products east of the crest (Poage and Chamberlain, 2002). Given that this time period coincides with marked global climate change (e.g. Raymo, 1994; Haug *et al*., 1999; Zachos *et al*., 2001), including the probable onset of glaciation in the Sierra, the apparent decrease in the rain shadow inferred from stable isotopes may result instead from poorly constrained climatic factors, such as changing storm tracks and/or the seasonality of precipitation over glacial–interglacial timescales, rather than decreasing crestal altitudes.

Discussion

Tectonic versus climatic forcing of incision

Distinguishing between tectonic and climatic forcing of erosion remains a key unresolved issue in geomorphic studies. The apparent pulse of incision in Sierra Nevada river canyons beginning *c*. 3 Ma could plausibly be due to either factor, as it coincides in time with both purported Pliocene uplift and marked changes in late Cenozoic climate (Zachos *et al*., 2001), including a major intensification of northern hemisphere glaciation. In fact, the erosional pulse could reflect any combination of the rock uplift pattern, a transient erosional response to rock uplift, or climate changes modulating river discharge and sediment supply.

Table V. Cosmogenic nuclide concentrations and bedrock erosion rates for Sierra Nevada interfluve surfaces[a]

Sample	Location	Altitude (m)	Latitude (°N)	^{26}Al (10^5 atom g^{-1})	^{10}Be (10^5 atom g^{-1})	^{26}Al/^{10}Be	^{26}Al erosion[b] (mm a^{-1})	^{10}Be erosion[b,c] (mm a^{-1})	^{26}Al age[d] (ka)	^{10}Be age[c,d] (ka)
HR-1	Hanging Rock	1975	36·53	42·85 ± 1·58	8·12 ± 0·18	5·28 ± 0·23	0·014 ± 0·003	0·013 ± 0·002	41·7 ± 9	45·7 ± 9
BR-1	Beetle Rock	1948	36·54	143·14 ± 4·96	28·17 ± 0·59	5·08 ± 0·21	0·004 ± 0·001	0·003 ± 0·001	144·6 ± 31	163·2 ± 34
BVD-1	Buena Vista Dome	2294	36·70	38·74 ± 1·35	6·85 ± 0·19	5·66 ± 0·25	0·020 ± 0·004	0·019 ± 0·004	29·3 ± 6	30·7 ± 6
DC-1	Markwood Meadow	1790	37·05	96·75 ± 3·03	18·71 ± 0·32	5·17 ± 0·18	0·006 ± 0·001	0·005 ± 0·001	91·9 ± 10	106·2 ± 11
Mean ± s.e.							0·011 ± 0·001	0·010 ± 0·001	76·9 ± 5·7	86·5 ± 6·4

[a] Some of these data were originally reported in Stock *et al.* (2004).
[b] Erosion rates calculated using Equation 1 assuming SLHL neutron production rates of $P_{26} = 31{\cdot}1$ atom g^{-1} a^{-1} and $P_{10} = 5{\cdot}1$ atom g^{-1} a^{-1} (Stone, 2000), and stopped muogenic production rates of $P_{26} = 0{\cdot}80$ atom g^{-1} a^{-1}, and $P_{10} = 0{\cdot}10$ atom g^{-1} a^{-1} (Heisinger *et al.*, 2002b). Production rates scaled for altitude and geographic latitude following Stone (2000) for neutrons and Granger *et al.* (2001a) for muons. Production rates and penetration depths corrected for geometric and depth shielding (Dunne *et al.*, 1999) and sample thickness. Uncertainties in erosion rates and effective exposure ages are propagated from analytical uncertainty, plus systematic uncertainties in production rates, attenuation coefficients, and radioactive decay constants.
[c] ^{10}Be erosion rates and effective ages are reported in text because ^{26}Al concentrations require measurement of stable ^{27}Al that introduces additional uncertainty.
[d] Effective timescales of erosion, given by $\Lambda\rho^{-1}\varepsilon^{-1}$.

Can climate change alone account for the variation in incision rates revealed by the dated caves? The onset of incision could plausibly be related to sudden enlargement of North American ice sheets around 2·5 to 2·7 Ma (e.g. Balco *et al*., 2005; Haug *et al*., 1999; Raymo, 1994). High-pressure systems resulting from these ice sheets are thought to have pushed the jet stream southward over the southern Sierra Nevada for much of the past 2·7 Ma, as apparently occurred during the Last Glacial Maximum (e.g. Bartlein *et al*., 1998). Increased precipitation accompanying this shift would amplify river discharge, thereby increasing Sierra Nevada river incision rates. Rapid river incision would progress until river profiles equilibrated to the new climate regime, after which time incision rates would slow (Whipple *et al*., 1999). However, climate records suggest that the progressive shift to colder and more variable climates has increased toward the present (e.g. Zachos *et al*., 2001), so climatically moderated discharge cannot fully explain the reduction in rates by 1·5 Ma. Glaciation of the headwaters provides a possible explanation. As the size and duration of glacial occupation increased during the Quaternary, glacial erosion of the headwaters decreased the overall slope of the river profile, thereby reducing stream power (Whipple *et al*., 1999). Canyon widening and deepening must have also produced prodigious sediment loads that were subsequently delivered to the fluvial system. This sediment may have inhibited bedrock incision if aggradation was sufficient to armour riverbeds against incision processes (e.g. Sklar and Dietrich, 1998; Whipple *et al*., 1999). Sediment aggradation would likely peak during glacial maxima, at the very time when river discharges would have been greatest (Hancock and Anderson, 2002). The shift from predominantly 41 ka to 100 ka glacial cycles at *c*. 1 Ma (Clark *et al*., 1999; Raymo, 1994) may have led to even larger glaciers and more prolonged sediment armouring downstream, further reducing incision after 1·5 Ma.

A tectonic mechanism for driving the pulse of incision is simpler, particularly if rock uplift occurred as a discrete event. Differential rock uplift would incite rapid incision as rivers responded to both increased slopes and increased discharge resulting from enhanced orographic precipitation. The onset of rapid incision at 3 Ma is broadly consistent with independent estimates of Sierra tectonism from *c*. 3·5 to 5 Ma (Huber, 1981; Unruh, 1991; Wakabayashi and Sawyer, 2001; Jones *et al*., 2004). If rivers responded to differential rock uplift from 3·5 to 5 Ma as a propagating wave of incision, then the pulse of incision midway up river profiles at 3 Ma is expected (Stock *et al*., 2004). Furthermore, a tectonic mechanism requires no switch in process to reduce bedrock incision after *c*. 1·5 Ma. Rather, the reduction would result either from waning rock uplift rates (reflecting both the duration of the delamination event, and the crustal response time to accomplish full flexural–isostatic compensation), or from a transient erosional event that passed the cave sites between 3 and 1·5 Ma (Stock *et al*., 2004). Although complicated tectonic–climate feedbacks ensure that the forcing must include some climatic component, we argue that the pulse of incision indicated by the caves reflects primary tectonic forcing in the form of a discrete Late Pliocene rock uplift event.

Mechanisms of rock uplift

Late Cenozoic relief production is the basis for proposed flexural–isostatic rock uplift of the range crest (Small and Anderson, 1995). Is the magnitude of late Cenozoic erosion and relief production sufficient to explain all of the observed tilt? Whipple *et al*. (1999) argued that a change to a more erosive climate should actually reduce relief, limiting the amount of flexural–isostatic rock uplift. However, they considered the steady-state case with hillslopes tightly coupled to rivers. In contrast, the Sierra Nevada, with incising river canyons separated by slowly eroding interfluves, appears to be in the midst of a transient erosional event, and is therefore a non-steady-state landscape. Inner gorge incision in the main stems is only slowly progressing into the interfluves; much of the broad upland surfaces are still effectively ignorant of main stem incision and are eroding at very low rates.

Slow erosion of broad interfluves dictates that flexural–isostatic rock uplift occur mainly through the deepening and widening of canyons (Jones *et al*., 2004). Although Quaternary glacial erosion in the High Sierra appears to have significantly altered basin hypsometry, relief is only slightly greater in this region than in non-glaciated drainages (Brocklehurst and Whipple, 2002). In fact, the greatest canyon relief in the southern Sierra lies in the non-glaciated regions (e.g. the confluence of Middle and South Fork Kings Rivers). Dated caves show that river canyons deepened by only *c*. 400 m in the past 3 Ma, and the presence of narrow inner gorges indicates minimal canyon widening during this time. Taken together, the considerable palaeorelief and moderate amounts of Late Pliocene incision suggest that late Cenozoic erosion alone is insufficient to drive all of the rock uplift inferred from tilted markers at the western edge of the range (Small and Anderson, 1995). This diminishes, but does not eliminate, the climatic effect on uplift, further strengthening the case for tectonically driven uplift. Delamination of eclogitic lithosphere beneath the Sierra appears to be a viable tectonic mechanism for inciting differential rock uplift in the late Cenozoic (Ducea and Saleeby, 1996; Jones *et al*., 2004). Although our data do not speak directly to the delamination mechanism, a pulse of incision midway up river profiles beginning *c*. 3 Ma coincides with postulated delamination at 3·5 Ma (Manley *et al*., 2000; Farmer *et al*., 2002; Jones *et al*., 2004), and the magnitude of canyon deepening at the cave sites is commensurate with the amount of rock uplift expected there based on crestal uplift estimates (Huber, 1981; Unruh, 1991; Wakabayashi and Sawyer, 2001). However, we stress that tectonic and climatic rock uplift mechanisms are not mutually exclusive. Whatever the initial driving mechanism, rock uplift accelerated river incision with respect to uplands, producing relief and inciting further rock uplift through flexural isostatic compensation.

Conclusions

Cosmogenic $^{26}Al/^{10}Be$ burial dating of cave sediment reveals that river incision in the Sierra Nevada was apparently slow (≤0·07 mm a^{-1}) from *c*. 4·7 to 3 Ma, accelerated to *c*. 0·3 mm a^{-1} between 3 and 1·5 Ma, and decreased thereafter to *c*. 0·02 mm a^{-1}. This pulse of incision created narrow inner gorges and deepened canyons by up to 500 m. However, inner gorges represent roughly only 20 per cent of the existing local relief, suggesting that, in the southern Sierra at least, much of the modern topography predated late Cenozoic uplift. Convexities in tributary streams suggest that rapid river incision midway up river profiles commenced at *c*. 3 Ma.

Concentrations of ^{26}Al and ^{10}Be in granitic interfluve surfaces indicate that upland surfaces are eroding at slow rates of *c*. 0·01 mm a^{-1}, a factor of two to three lower than incision in the adjacent canyons over equivalent time periods, and more than an order of magnitude less than late Pliocene incision. Although local relief likely declined throughout much of the Cenozoic, the discrepancy between river incision rates and upland erosion rates over the past *c*. 3 Ma demonstrates an increase in local relief during this time. The erosional pulse in the trunk rivers is translating slowly up tributary streams, isolating uplands from the effects of uplift and preserving much of the early Cenozoic landscape. Low spatially averaged erosion rates have acted to preserve the broad topographic form of the Sierra Nevada for much of the Cenozoic.

Persistent high altitudes and local relief during the early Cenozoic need not preclude renewed uplift and erosion in the Pliocene. Rapid incision beginning *c*. 3 Ma coincides with estimates of renewed tectonism (Unruh, 1991; Wakabayashi and Sawyer, 2001; Jones *et al*., 2004), and may represent the erosional response to rock uplift associated with delamination of the batholithic root (Manley *et al*., 2000; Jones *et al*., 2004). Considerable pre-Pliocene relief, modest Pliocene inner gorge development, and low rates of upland erosion together suggest that the flexural isostatic response to late Cenozoic erosion is probably not sufficient to drive all of the rock uplift documented by tilted markers. We therefore favour a tectonic mechanism, such as root delamination, for inciting uplift, but do recognize the contribution of flexural–isostatic uplift to the total rock uplift.

Acknowledgements

We thank Joel Despain and Steve Bumgardner for field assistance, and Sequoia and Kings Canyon National Parks and Sequoia National Forest for permission to collect samples. Darryl Granger provided guidance with cosmogenic chemistry. We appreciate discussions with William Bull, Darryl Granger, Paul Koch, Christina Ravelo, John Wakabayashi, and the participants of the 2003 Pacific Cell Friends of the Pleistocene field trip. William Bull, Eric Kirby, and an anonymous reviewer provided helpful comments. This research was funded by grants from the National Science Foundation (EAR-0126253) and the Institute of Geophysics and Planetary Physics. Cosmogenic nuclide measurements were performed under the auspices of the US Department of Energy by the University of California, Lawrence Livermore National Laboratory, under contract W-7405-Eng-48.

References

Ague JJ, Brimhall GH. 1988. Magmatic arc asymmetry and distribution of anomalous plutonic belts in the batholiths of California: Effects of assimilation, crustal thickness, and depth of crystallization. *Geological Society of America Bulletin* **100**: 912–927.

Anderson RS. 2002. Modeling the tor-dotted crests, bedrock edges, and parabolic profiles of high alpine surfaces of the Wind River Range, Wyoming. *Geomorphology* **46**: 35–58.

Anderson RS, Repka JL, Dick GS. 1996. Explicit treatment of inheritance in dating depositional surfaces using in situ ^{10}Be and ^{26}Al. *Geology* **24**: 47–51.

Balco G, Rovey II CW, Stone JOH. 2005. The first glacial maximum in North America. *Science* **307**: 222.

Bartlein PJ, Anderson KH, Anderson PM, Edwards ME, Mock CJ, Thompson RS, Webb III T, Whitlock C. 1998. Paleoclimate simulations for North America over the past 21 000 years: Features of the simulated climate and comparisons with paleoenvironmental data. *Quaternary Science Reviews* **17**: 549–585.

Bateman PC, Wahrhaftig C. 1966. Geology of the Sierra Nevada. In *Geology of Northern California*, Bailey EH (ed.). *California Division of Mines and Geology Bulletin* **190**: 107–172.

Bierman PR. 1994. Using in situ produced cosmogenic isotopes to estimate rates of landscape evolution: A review from the geomorphic perspective. *Journal of Geophysical Research* **99**: 13 885–13 896.

Bierman PR, Caffee M. 2002. Cosmogenic exposure and erosion history of Australian bedrock landforms. *Geological Society of America Bulletin* **114**: 787–803.

Bierman PR, Steig E. 1996. Estimating rates of denudation and sediment transport using cosmogenic isotope activities in sediment. *Earth Surface Processes and Landforms* **21**: 125–139.

Brocklehurst SH, Whipple KX. 2002. Glacial erosion and relief production in the Eastern Sierra Nevada, California. *Geomorphology* **42**: 1–24.

Brown ET, Stallard RF, Larsen MC, Raisbeck GM, Yiou F. 1995. Denudation rates determined from the accumulation of in situ-produced cosmogenic nuclides. *Earth and Planetary Science Letters* **124**: 19–33.

Bull WB. 1991. *Geomorphic Responses to Climate Change*. Oxford University Press: London.

Burbank DW, Leland J, Fielding E, Anderson RS, Brozovic N, Reid MR, Duncan C. 1996. Bedrock incision, rock uplift, and threshold hillslopes in the northwestern Himalayas. *Nature* **379**: 505–510.

Chamberlain CP, Poage MA. 2000. Reconstructing the paleotopography of mountain belts from the isotopic composition of authigenic minerals. *Geology* **28**: 115–118.

Chen JH, Moore JG. 1982. Uranium-lead isotopic ages from the Sierra Nevada batholith. *Journal of Geophysical Research* **87**: 4761–4784.

Clark PU, Alley RB, Pollard D. 1999. Northern Hemisphere ice-sheet influences on global climate change. *Science* **286**: 1104–1111.

Dalrymple GB. 1963. Potassium-Argon dates of some Cenozoic volcanic rocks of the Sierra Nevada, California. *Geological Society of America Bulletin* **74**: 379–390.

Dalrymple GB. 1964. Cenozoic chronology of the Sierra Nevada, California. *University of California Publications in Geological Sciences* **47**: 1–41.

Ducea MN, Saleeby JB. 1996. Buoyancy sources for a large, unrooted mountain range, the Sierra Nevada, California: Evidence from xenolith thermobarometry. *Journal of Geophysical Research* **101**: 8229–8244.

Ducea MN, Saleeby JB. 1998. A case for delamination of the deep batholithic crust beneath the Sierra Nevada. *International Geology Review* **40**: 78–93.

Dunne J, Elmore D, Muzikar P. 1999. Scaling factors for the rates of production of cosmogenic nuclides for geometric shielding and attenuation at depth on sloped surfaces. *Geomorphology* 27: 3–11.

Farmer GL, Glazner AF, Manley CR. 2002. Did lithospheric delamination trigger late Cenozoic potassic volcanism in the southern Sierra Nevada, California? *Geological Society of America Bulletin* **114**: 754–768.

Granger DE, Muzikar PF. 2001. Dating sediment burial with in situ-produced cosmogenic nuclides: Theory, techniques, and limitations. *Earth and Planetary Science Letters* **188**: 269–281.

Granger DE, Kirchner JW, Finkel RC. 1996. Spatially averaged long-term erosion rates measured from in situ-produced cosmogenic nuclides in alluvial sediment. *Journal of Geology* **104**: 249–257.

Granger DE, Kirchner JW, Finkel RC. 1997. Quaternary downcutting rate of the New River, Virginia, measured from differential decay of cosmogenic ^{26}Al and ^{10}Be in cave-deposited alluvium. *Geology* **25**: 107–110.

Granger DE, Riebe CS, Kirchner JW, Finkel RC. 2001a. Modulation of erosion on steep granitic slopes by boulder armoring, as revealed by cosmogenic ^{26}Al and ^{10}Be. *Earth and Planetary Science Letters* **186**: 269–281.

Granger DE, Fabel D, Palmer AN. 2001b. Pliocene-Pleistocene incision of the Green River, Kentucky, determined from radioactive decay of cosmogenic ^{26}Al and ^{10}Be in Mammoth Cave sediments. *Geological Society of America Bulletin* **113**: 825–826.

Hancock GS, Anderson RS. 2002. Numerical modeling of fluvial terrace formation in response to oscillating climate. *Geological Society of America Bulletin* **114**: 1131–1142.

Hancock GS, Anderson RS, Chadwick OA, Finkel RC. 1999. Dating fluvial terraces with ^{10}Be and ^{26}Al profiles: Application to the Wind River, Wyoming. *Geomorphology* **27**: 41–60.

Hanks TC, Lucchitta I, Davis SW, Davis ME, Finkel RC, Lefton SA, Garvin CD. 2004. The Colorado River and the age of Glen Canyon. In *The Colorado River: Origin and Evolution*, Young RA, Spamer EE (eds). Grand Canyon Association Monograph **12**: 129–133.

Haug GH, Sigman DM, Tiedemann R, Pedersen TF, Sarnthein M. 1999. Onset of permanent stratification in the subarctic Pacific Ocean. *Nature* **401**: 779–782.

Heisinger B, Lal D, Jull AJT, Kubik S, Ivy-Ochs S, Neumaier S, Knie K, Lazarev V, Nolte E. 2002a. Production of selected cosmogenic radionuclides by muons: 1. Fast muons. *Earth and Planetary Science Letters* **200**: 345–355.

Heisinger B, Lal D, Jull AJT, Kubik S, Ivy-Ochs S, Knie K, Nolte E. 2002b. Production of selected cosmogenic radionuclides by muons: 2. Capture of negative muons. *Earth and Planetary Science Letters* **200**: 357–369.

House MA, Wernicke BP, Farley KA. 1998. Dating topography of the Sierra Nevada, California, using apatite (U-Th)/He ages. *Nature* **396**: 66–69.

House MA, Wernicke BP, Farley KA. 2001. Paleo-geomorphology of the Sierra Nevada, California, from (U-Th)/He ages in apatite. *American Journal of Science* **301**: 77–102.

Huber NK. 1981. *Amount and timing of Late Cenozoic uplift and tilt of the central Sierra Nevada, California – evidence from the upper San Joaquin river basin*. US Geological Survey Professional Paper 1197.

Jones CH, Farmer GL, Unruh J. 2004. Tectonics of Pliocene delamination of lithosphere of the Sierra Nevada, California. *Geological Society of America Bulletin* **116**: 1408–1422.

Kohl CP, Nishiizumi K. 1992. Chemical isolation of quartz for measurement of *in-situ*-produced cosmogenic nuclides. *Geochimica et Cosmochimica Acta* **56**: 3583–3587.

Lal D. 1991. Cosmic ray labeling of erosion surfaces: In situ nuclide production rates and erosion models. *Earth and Planetary Science Letters* **104**: 424–439.

Lave J, Avouac JP. 2000. Active folding of fluvial terraces across the Siwalik Hills, Himalaya of central Nepal. *Journal of Geophysical Research* **105**: 5735–5770.

Lindgren W. 1911. *The Tertiary gravels of the Sierra Nevada of California*. US Geological Survey Professional Paper 73.

Manley CR, Glazner AF, Farmer GL. 2000. Timing of volcanism in the Sierra Nevada of California: Evidence for Pliocene delamination of the batholithic root? *Geology* **28**: 811–814.

Masarik J, Reedy RC. 1995. Terrestrial cosmogenic nuclide production systematics calculated from numerical simulations. *Earth and Planetary Science Letters* **136**: 381–395.

Matthes FE. 1960. *Reconnaissance of the geomorphology and glacial geology of the San Joaquin Basin, Sierra Nevada, California*. US Geological Survey Professional Paper 329.

Matthes FE. 1965. *Glacial Reconnaissance of Sequoia National Park, California*. US Geological Survey Professional Paper 504-A.

Middleton R, Brown L, Desfouly-Arjomandy B, Klein J. 1993. On ^{10}Be standards and the half-life of ^{10}Be. *Nuclear Instruments and Methods in Physics Research B* **82**: 399–403.

Molnar P, England P. 1990. Late Cenozoic uplift of mountain ranges and global climate change: Chicken or egg? *Nature* **346**: 29–34.

Nishiizumi K, Winterer EL, Kohl CP, Klein J, Middleton R, Lal D, Arnold JR. 1989. Cosmic ray production rates of ^{10}Be and ^{26}Al in quartz from glacially polished rocks: *Journal of Geophysical Research* **94**: 17907–17915.

Norris TL, Gancarz AJ, Rokop DJ, Thomas KW. 1983. Half-life of ^{26}Al: Proceedings of the Fourteenth Lunar and Planetary Science Conference, Part I. *Journal of Geophysical Research* **88**: B331–B333.

Palmer AN. 1987. Cave levels and their interpretation. *National Speleological Society Bulletin* **49**: 50–66.

Palmer AN. 1991. Origin and morphology of limestone caves. *Geological Society of America Bulletin* **103**: 1–21.

Partridge TC, Granger DE, Caffee MW, Clarke RJ. 2003. Lower Pliocene Hominid remains from Sterkfontein. *Science* **300**: 607–612.

Poage MA, Chamberlain CP. 2002. Stable isotopic evidence for a pre-middle Miocene rain shadow in the western Basin and Range: Implications for the paleotopography of the Sierra Nevada. *Tectonics* **21**: 1601–1610.

Raymo ME. 1994. The initiation of Northern Hemisphere glaciation. *Annual Reviews of Earth and Planetary Sciences* **22**: 353–383.

Raymo ME, Ruddiman WF. 1992. Tectonic forcing of late Cenozoic climate. *Nature* **359**: 117–122.

Reusser LJ, Bierman PR, Pavich MJ, Zen E, Larsen J, Finkel R. 2004. Rapid late Pleistocene incision of Atlantic passive-margin river gorges. *Science* **305**: 499–502.

Riebe CS, Kirchner JW, Granger DE, Finkel RC. 2000. Erosional equilibrium and disequilibrium in the Sierra Nevada, inferred from cosmogenic ^{26}Al and ^{10}Be in alluvial sediment. *Geology* **28**: 803–806.

Riebe CS, Kirchner JW, Granger DE, Finkel RC. 2001. Minimal climatic control of erosion rates in the Sierra Nevada, California. *Geology* **29**: 447–450.

Ruppert S, Fliedner MM, Zandt G. 1998. Thin crust and active upper mantle beneath the southern Sierra Nevada in the western United States. *Tectonophysics* **286**: 237–252.

Saleeby J, Ducea M, Clemens-Knott D. 2003. Production and loss of high-density batholithic root, southern Sierra Nevada, California. *Tectonics* **22** 1604.001: 10.1029/2002TC001374.

Schaller M, von Blanckenburg F, Hovius N, Kubik PW. 2001. Large scale erosion rates from *in situ*-produced cosmogenic nuclides in European river sediments. *Earth and Planetary Science Letters* **188**: 441–458.

Schaller M, von Blanckenburg F, Veldkamp A, Tebbens LA, Hovius N, Kubik PW. 2002. A 30 000 a record of erosion rates from cosmogenic ^{10}Be in Middle European river terraces. *Earth and Planetary Science Letters* **204**: 307–320.

Sklar LS, Dietrich WE. 1998. River longitudinal profiles and bedrock incision models: Stream power and the influence of sediment supply. In *Rivers Over Rock: Fluvial Processes in Bedrock Channels*, Tinkler KJ, Wohl EE. (eds). American Geophysical Union: Washington DC; 237–260.

Small EE, Anderson RS. 1995. Geomorphically driven Late Cenozoic rock uplift in the Sierra Nevada, California. *Science* **270**: 277–280.

Small EE, Anderson RS. 1998. Pleistocene relief production in Laramide mountain ranges, western United States. *Geology* **26**: 123–126.

Small EE, Anderson RS, Repka JL, Finkel R. 1997. Erosion rates of alpine bedrock summit surfaces deduced from in situ ^{10}Be and ^{26}Al. *Earth and Planetary Science Letters* **150**: 413–425.

Stock GM, Anderson RS, Finkel RC. 2004. Pace of landscape evolution in the Sierra Nevada, California, revealed by cosmogenic dating of cave sediments. *Geology* **32**: 193–196.

Stone JO. 2000. Air pressure and cosmogenic isotope production. *Journal of Geophysical Research* **105**: 23753–23759.

Unruh JR. 1991. The uplift of the Sierra Nevada and implications for Late Cenozoic epeirogeny in the western Cordillera. *Geological Society of America Bulletin* **103**: 1395–1404.

Vance D, Bickle M, Ivy-Ochs S, Kubick PW. 2003. Erosion and exhumation in the Himalaya from cosmogenic isotope inventories of river sediments. *Earth and Planetary Science Letters* **206**: 273–288.

Wakabayashi J, Sawyer TL. 2001. Stream incision, tectonics, uplift, and evolution of topography of the Sierra Nevada, California. *Journal of Geology* **109**: 539–562.

Wernicke B, Clayton R, Ducea M, Jones CH, Park S, Ruppert S, Saleeby J, Snow JK, Squires L, Fliedner M, Jiracek G, Keller R, Klemperer S, Luetgart J, Malin P, Miller K, Mooney W, Oliver H, Phinney R. 1996. Origin of high mountains in the continents: The southern Sierra Nevada. *Science* **271**: 190–193.

Whipple KX, Tucker GE. 1999. Dynamics of the stream power river incision model: Implications for the height limits of mountain ranges, landscape response timescales, and research needs. *Journal of Geophysical Research* **104**: 17661–17674.

Whipple KX, Kirby E, Brocklehurst SH. 1999. Geomorphic limits to climate induced increases in topographic relief. *Nature* **401**: 39–43.

Wolkowinsky AJ, Granger DE. 2004. Early Pleistocene incision of the San Juan River, Utah, dated with ^{26}Al and ^{10}Be. *Geology* **32**: 749–752.

Zachos J, Pagani M, Sloan L, Thomas E, Billups K. 2001. Trends, rhythms, and aberrations in global climate 65 Ma to present. *Science* **292**: 686–693.

Zhang P, Molnar P, Downs WR. 2001. Increased sedimentation rates and grain sizes 2–4 Myr ago due to the influence of climate change on erosion rates. *Nature* **410**: 891–897.

